HHS Public Access

Author manuscript

Biochemistry. Author manuscript; available in PMC 2016 March 03.

Published in final edited form as:

Biochemistry. 2015 March 3; 54(8): 1589–1599. doi:10.1021/bi501376f.

Conditional Trimerization and Lytic Activity of HIV-1 gp41 Variants containing the Membrane-Associated Segments

Zhou Dai, **Yisong Tao**, **Nina Liu**, **Michael D. Brenowitz**, **Mark E. Girvin**, and **Jonathan R. Lai***

Department of Biochemistry, Albert Einstein College of Medicine, 1300 Morris Park Avenue, Bronx, NY 10461

Abstract

Fusion of host and viral membranes is a critical step during infection by membrane-bound viruses. The HIV-1 glycoproteins gp120 (surface subunit) and gp41 (fusion subunit) represent the prototypic system for studying this process; in the prevailing model, the gp41 ectodomain forms a trimeric six-helix bundle that constitutes a critical intermediate and provides the energetic driving for overcoming barriers associated with membrane fusion. However, most structural studies of gp41 variants have been performed either on ectodomain constructs lacking one or more of membrane-associated segments (the fusion peptide, FP, the membrane-proximal external region, MPER, and transmembrane domain, TM), or on variants consisting of these isolated segments alone without the ectodomain. Several recent reports have suggested that the HIV-1 ectodomain, as well as larger construct containing the membrane-bound segments, dissociate from a trimer to a monomer in detergent micelles. Here we compare the properties of a series of gp41 variants to delineate the roles of the ectodomain, FP, and MPER and TM, all in membrane-mimicking environments. We find that these proteins are prone to formation of a monomer in detergent micelles. In one case, we observed exclusive monomer formation at pH 4 but conditional trimerization at pH 7 even at low micromolar (~5 μM) protein concentrations. Liposome release assays demonstrate that these gp41-related proteins have the capacity to induce content leakage, but that this activity is also strongly modulated by pH with much higher activity at pH 4. Circular dichroism, NMR, and binding assays with antibodies specific to the MPER provide insight into the structural and functional roles of the FP, MPER, and TM and their effect on structure within the larger context of the fusion subunit.

Infection by enveloped viruses requires fusion of the host and viral membranes, a process that is facilitated by the envelope glycoprotein. Although the details vary among viruses and structural classes (Class I, α-helical; class II, β-sheet; or class III, mixed α/β structure), the general aspects are conserved and involve three distinct conformations of the envelope

*To whom correspondence should be addressed: jon.lai@einstein.yu.edu. Phone: 718-430-8641. Fax: 718-430-8565.

SUPPORTING INFORMATION **AVAILABLE**

Figure S1 shows liposomal release assay for various gp41 constructs. Figure S2 shows AUC data for gp41-shortNC$^{\Delta FP}$ and gp41-MTC. Figure S3 shows representative binding data between bNAbs 2F5 and 4E10 with gp41 constructs. Table S1 shows the effect of GdnHCl on DPC micelle diameter. This material is available free of charge via the Internet at http://pubs.acs.org.

CONFLICT OF INTEREST STATEMENT

The authors declare no competing financial interest.

glycoprotein: a prefusion form, an extended or “prehairpin” intermediate, and a stable post-fusion form. The HIV-1 envelope glycoproteins gp120 and gp41 are perhaps the most well studied viral fusion proteins.[1–6] The fusion pathway (Figure 1) typifies the class I mechanism and is typically drawn with gp120 and gp41 forming a trimer of heterodimers in the prefusion conformation. Interaction of gp120 with CD4 and coreceptors (CXCR4 or CCR5) results in a conformational change in gp41 such that the N-terminal fusion peptide is extended into the host cell membrane to create the extended intermediate.[2,4] Next, formation of a six-helix bundle by the N- and C-terminal heptad repeat regions (NHR and CHR) of the gp41 ectodomain promotes initial fusion events that ultimately lead to coalescence of the viral and host cell membranes. Formation of a fusion pore allows transfer of the viral genetic contents into the host cell, and this is promoted by formation of the post-fusion six-helix bundle.

Fusion of two lipid bilayers is a thermodynamically favorable but there is a high kinetic barrier (40–50 kcal/mol) associated with bringing the two phospholipid surfaces into proximity and introducing local deformations in the membrane required for initial lipid mixing events.[2–4] It is argued that the energy released from folding of the fusion subunit (gp41 in HIV-1) six-helix bundle is required to overcome the membrane fusion barrier. Although there is general agreement with this model, the evidence for it is largely indirect. The hypothesized extended intermediate conformation of gp41 has never been visualized in high- or low-resolution.[7,8] Furthermore, there are experimental observations that formation of the six-helix bundle does not occur concomitantly with hemifusion (mixing of the outer two bilayers) but rather at some point later in fusion.[9] Fusion inhibitors and immunogens that mimic conformational intermediates of the fusion pathway are subjects of intense therapeutic and vaccine development campaigns. Therefore, understanding atomic details of HIV-1 gp41-mediated membrane fusion is of both basic and translational importance.

Most structural studies on gp41 to date (alone or in the context of the prefusion spike) have involved either isolated ectodomain segments (i.e., NHR, CHR, and intervening loop) or the isolated membrane segments (fusion peptide, FP, membrane-proximal external region, MPER, and transmembrane domain, TM).[1,5,6,10–16] A handful of studies have focused on larger combinations of membrane and ectodomain segments; characterization of these variants has yielded some surprising results. Weliky and coworkers have demonstrated that constructs consisting of the FP, NHR, and CHR exhibit pH-dependent fusion activity.[13,15,17] More recently, this group reported that the dominant state of a gp41 ectodomain construct was a monomer at low pH (pH 3.2) in the absence of guanadinium hydrochlodride (GdnHCl), but a hexamer at either pH 3.2 or pH 7.4 in the presence of 6 M GdnHCl.[18] Bax and coworkers have shown that a construct consisting of the FP, NHR, immunodominant loop, CHR, MPER and TM form complete trimers in n-dodecylphosphocholine (DPC) micelles but only at high concentrations (hundreds of micromolar).[19] Similar results have been reported by the Wingfield and Tamm groups on a similar gp41 construct but lacking the FP segment.[20,21] Furthermore, the ectodomain NHR/CHR segments themselves undergo dissociation from the canonical trimer to a structured but dynamic monomer in the presence of DPC micelles.[12] These insights have led to a newer molecular model for membrane fusion in which dissociation of the core NHR/CHR trimer represents a novel “monomeric” or “dissociated” intermediate in the fusion pathway (Figure 1A).[12] However, the precise role

of this monomeric/dissociated intermediate, and which fusion-related activities may result from it, remain to be established.

Here we describe biochemical studies on several gp41 variants containing different combinations of the ectodomain and membrane segments to understand the role of each individual element. We find, in agreement with recent studies, that the fusion subunit has the capacity to dissociate into monomers in detergent environments. In one case, we discovered that the trimer to monomer dissociation is induced by low pH. Furthermore, we found that these membrane-bound gp41 proteins induce leakage from liposomes, suggesting fusogenic activity, but that this lytic activity is affected by pH with higher activity at pH 4 and strongly attenuated activity at pH 7. Subsequent CD and binding studies with antibodies against the MPER provide additional insight into the structural and functional roles of the membrane-bound segments.

MATERIALS AND METHODS

Protein Expression and Purification

Synthetic DNA fragments encoding gp41 constructs (described in the Results section) were obtained from a commercial supplier (Genewiz, South Plainfield, NJ). These gp41 construct genes were cloned into expression vector pET-22b(+) (Novagen, Billerica, MA). Protein expression for these constructs was screened using several *E. coli* strains: BL21(DE3) (New England Biolabs, Ipswich, MA), Lemo21(DE3) (New England Biolabs, Ipswich, MA), BL21-AI (Life Technologies, Carlsbad, CA), C41(DE3) (Lucigen Corporation, Middleton, WI), C41(DE3)-pLysS (Lucigen Corporation, Middleton, WI), C43(DE3) (Lucigen Corporation, Middleton, WI) and C43(DE3)-pLysS (Lucigen Corporation, Middleton, WI)). BL21(DE3) cells provided the highest expression of gp41-longNC while Lemo21(DE3) cells provided the highest expression for all other constructs. For all constructs, cell culture was grown to OD_{600nm} ~ 0.5 at 37 °C and induced with 0.5 mM isopropyl β-D-1-thiogalactopyranoside (IPTG) at 22 °C. After 16–20 hours expression, cells were pelleted with centrifugation. The expressed cell pellet was first lysed with BugBuster (EMD Millipore, Billerica, MA) lysis buffer in phosphate buffered saline (PBS, pH 7.0) and the lysate pellet which contains gp41 protein as inclusion bodies was washed three times with PBS. The washed pellet was then solublized with PBS containing 0.2% SDS and 8 M urea. Solublized gp41 proteins were purified through Ni-NTA (Ni-Nitrilotriacetic acid agarose, QIAGEN, Valencia, CA) column, and folded by exchanging SDS with n-dodecylphosphocholine (DPC, Avanti Polar Lipids, Alabaster, AL) on the column. After purification, gp41 proteins were characterized in 20 mM sodium phosphate buffer with 0.5% DPC at pHs 6–8 or in 20 mM sodium acetate buffer with 0.5% DPC at pHs 4–5.

Circular Dichroism

Circular dichroism (CD) measurements were performed on a Jasco J-815 spectrometer with a 1 cm quartz cuvette for the full-wavelength spectra and chemical denaturation experiments. Protein concentrations for CD ranged from 1 to 2 μM, as determined by the absorbance at 280 nm. Full wavelength spectra were obtained with a 0.5 nm step size and represent the average of three scans. The signal was converted to mean molar ellipticity (θ)

using the equation: θ (in deg cm^2 $dmol^{-1}$) = millidegrees/(pathlength in millimeters × the molar protein concentration × the number of residues). 0–7 M guanidinium hydrochloride (GdnHCl) was used for chemical denaturation of gp41 constructs. The denaturation was monitored at 222 nm (θ_{222}) at 22 °C. Estimation of secondary structure content was performed by the K2D3 program.[22]

Analytical Ultracentrifugation

A sedimentation velocity study of the gp41 constructs was conducted using the absorption optics of a Beckman Optima XL-I analytical ultracentrifuge with samples loaded into two-sector cell assemblies run in the AN-60Ti rotor. Boundary movement was followed at 280 nm during centrifugation at 58,000 rpm and 20 °C in buffer containing 20 mM sodium phosphate, 150 mM NaCl buffer with 0.5% DPC at pHs 6, 7 and 8, and 20 mM sodium acetate, 150 mM NaCl with 0.5% DPC at pHs 4 and 5. D_2O was used to density match the DPC present in the buffer.[23–25] Sixty to 70 scans were typically collected over the course of the sedimentation run of which a subset, beginning with those where a clear plateau is evident between the meniscus and the boundary, was selected for time-derivative analysis using DCDT+ version 2.4.2 by John Philo.[26,27] The extinction coefficient at 280 nm was calculated from the protein sequences using ExPASy. Protein concentrations ranging from 4 to 16 μM were analyzed, and the corresponding buffer was used to blank each sample. Values of the buffer density and viscosity were calculated from the composition (neglecting the detergent) using Sedenterp version 20120828 Beta (http://sednterp.unh.edu/#). The partial specific volume of the gp41 construct was calculated from its sequence also using Sedenterp. The sedimentation parameters were corrected to standard conditions (20, w) using these values.

Liposomal Release Assays

Fluorescent dye 8-aminonapthalene-1,3,6 trisulfonic acid (ANTS) and its quencher *p*-xylene-bis-pyridinium bromide (DPX) were co-encapsulated in POPC/POPG (POPC, 1-palmitoyl-2-oleoyl-sn-glycero-3-phosphocholine; POPG, 1-palmitoyl-2-oleoyl-sn-glycero-3-phosphoglycerol; Avanti Polar Lipids) (4:1, molar ratio) liposomes. 10 cycles of Freeze/thaw process and 11 rounds of extrusion with 100 nm membrane were performed to generate homogenous large unilamellar vesicles. Next, a 10 mL Sepharose CL-2B size exclusion column was used to isolate liposomes with encapsulated ANTS/DPX for the following assays.

An Infinite M1000 PRO plate reader was used to monitor liposomal content release induced by gp41 constructs. Excitation was at 355 nm with an 8 nm slit width, and emission was monitored at 520 nm with a 12 nm slit width. The stock protein solutions used for the leakage assay were pre-adjusted to the corresponding pHs and 4 μM protein concentration. Varying concentrations of gp41 proteins were added to ANTS/DPX-encapsulated liposomes to test for their fusion activity. Addition of extra amount of Zn^{2+} was used to coordinate histidine tags within the proteins and to remove potential leakage effects from the tags. Buffer with 0.005% DPC was used as baseline (0% content release), while buffer with 0.3% triton was used as 100% content release.

Nuclear Magnetic Resonance

Minimal media (M9) with $^{15}NH_4Cl$ was used for expressing gp41-shortNC and gp41-longNC. The ^{15}N labeled gp41 proteins were purified using the same protocol as unlabeled proteins. After purification, the protein samples were concentrated to ~100 μM for NMR measurements at pH 4. NMR experiments were carried out on a Bruker Avance III 600 MHz spectrometer using a Cryo-TCI probe. All TROSY-HSQC were acquired at 37°C for 3.5 hours with a maximum acquisition time of 66 ms in t_1 and 95 ms in t_2. Data were processed with a Gaussian filter with a baseline correction in both dimensions using NMRPipe.[28] Referencing was made with respect to 4,4-dimethyl-4-silapentane-1-sulfonic acid (DSS).

Biolayer Interferometry

The forteBio BLItz system was used to determine the binding properties of gp41 constructs with HIV-1 gp41 monoclonal antibodies 2F5 and 4E10. Anti-human Fc capture sensors were used for initial antibody (2F5 or 4E10) loading, which was followed by gp41 proteins association and dissociation analysis. 10 and 100 μg/mL antibody were used for loading at pH 7 and 4, respectively. The measurements for both gp41 association and dissociation were performed in buffers containing 0.1% DPC. For each gp41 construct, at least three different concentrations, varying from 0.1 μM to 10 μM, were used, and subsequently global fitting was used to generate the k_a (association rate constant), k_d (dissociation rate constant) and K_D (equilibrium dissociation constant) values.

RESULTS

Protein Design, Expression, and Purification

The proteins characterized in this study are shown in Figure 2. We focused our designs on residues 512–715 of the Env precursor (HxB2 numbering), which contains all the fusion-relevant portions and encompasses the FP (512–541), the NHR (542–581), immunodominant loop (582–627), CHR (628–664), MPER (665–683), TM domain (684–711), and four residues of the C-terminal tail (712–715). The construct “gp41-longNC” consists of all the membrane segments and the intervening ectodomain but with a short polypeptide linker (~SGGRGG~) replacing the immunodominant loop. A number of studies have shown that behavior of the NHR and CHR segments in the absence or presence of detergent is similar in constructs containing or lacking the immunodominant loop.[12–15,29] The construct “gp41-shortNC” also contains full membrane segments but with significantly shorter segments of the NHR and CHR, joined by a ~GSWGG~ linker. This design was intended to retain minimal portions of the NHR and CHR, potentially in an α-helical conformation, but reduce its contribution to structure and stability while retaining the full membrane-active behavior. When compared to the crystal structure of the “post-fusion” ectodomain,[1,5] the NHR and CHR segments in gp41-shortNC encompass ~4 and 4.5 α-helical turns each. Two deletion mutants, gp41-shortNC$^{\Delta FP}$ and gp41-shortNC$^{\Delta MTC}$ lack the FP and MPER-TM-C regions, respectively, and were intended to explore role of interactions between the FP and MPER-TM segments in structural stability and fusion activity. Finally, a construct consisting of the MPER, TM, and C segments (gp41-MTC) was also examined, and is similar to the MPER-TM1 protein previously studied by Scott and coworkers.[10] All constructs contain N- and C-terminal hexahistidine tags. Proteins were expressed in *E. coli*

and purified from inclusion bodies, with the presence SDS required to maintain solubility throughout the purification. Refolding was accomplished by on-column buffer exchange into buffer containing 0.5% DPC.

Structural and Functional Properties of gp41-longNC and gp41-shortNC

Circular dichroism (CD) revealed that both gp41-longNC and gp41-shortNC are α-helical across a broad pH range, evident by characteristic double minima wavelength spectra (Figures 3A and 4A). That the proteins do not precipitate over this pH range and remain α-helical indicates that their secondary structure does not change over the pH range analyzed. The CD spectra predict α-helical content of 70% for gp41-longNC. The prediction is 44% α-helical for gp41-shortNC, which is consistent with the smaller length of the helical NHR and CHR, with some additional fraying near the connecting linker. To determine whether the short construct retains the structural features of the gp41-longNC, both proteins were produced in ^{15}N-labeled form and their ^{1}H^{15}N TROSY spectra recorded (Figure 5). Consistent with previous studies on gp41$^{1–194}$ and gp41$^{27–194}$ constructs,[19,20] we found the solubility and stability of gp41-longNC and gp41-shortNC to be greatest at pH 4 and spectra were recorded under these conditions. In particular, gp41-longNC was prone to precipitation at concentrations higher than ~20 μM at pH 7, but stable at 120 μM at pH 4, in accordance with observations that gp41 constructs containing the ectodomain and FP having higher solubility in acidic pH environments.[18,30,31] The ^{1}H^{15}N TROSY spectra of both proteins showed the modest spectral dispersion typical of α-helical proteins (Figure 5), suggesting that both were well folded, with considerable α-helical content. The chemical shifts for gp41-longNC are quite similar to those previously reported for a similar construct.[19] Of the 95 resolvable cross-peaks for gp41-shortNC, 85 nearly overlap with the corresponding cross-peaks in gp41-longNC, indicating that the gp41-shortNC construct is folded with a structure similar to the gp41-longNC construct.

Sedimentation velocity experiments conducted at 4 – 5 μM protein concentrations and at pHs 4 and 8 revealed surprisingly that gp41-longNC undergoes a pH-dependent monomer-to-trimer assembly. The s* distribution at high and low pH is well described as a single component (Figure 3B). $S_{20,w}$ and apparent M_w (S/D) values of 1.352 (68.3% confidence limits: 1.349, 1.354) *S* and 19.5 (19.3, 19.7) kDa and 3.309 (3.298, 3.319) *S* and 62.1 (58.7, 65.5) kDa were measured at pH 4 and pH 8, respectively. The *S* and apparent M_w values are consistent with gp41-longNC shifting from monomer to trimer as a function of pH (calculated M_w values are 21.7 and 65.1 kDa, respectively). Furthermore, gp41-longNC is a stable trimer from pH 8 to 6 at the 4 – 5 μM protein concentrations used in the experiments (Figure 3B). At pH 5.0, a bimodal s* distribution is observed that is well described by a constrained monomer to trimer assembly with $S_{20,w}$ (S/D) values of 1.514 (1.507, 1.519) *S* and 3.024 (3.024, 3.027) *S* respectively, and apparent M_w of 21.5 (21.0, 21.8) kDa for monomer. This result is consistent with equilibration of monomer and trimer being slow relative to the sedimentation rate and thus appropriately modeled as the sum of two independent components. Confirmation of this conclusion was obtained by conducting additional sedimentation studies at higher and lower protein concentrations. Bimodal distributions are again observed with the higher *S* component (trimer) increasing with increasing protein concentration (data not shown). Taken together these results confirm that

gp41-longNC is in a slowly equilibrating reversible monomer-trimer assembly reaction in solution.

In contrast, the s* distribution obtained for gp41-shortNC at concentrations ranging from 5 to 21 μM at pH 7 is best described as monomer with a very small fraction (3.6%) of trimer with $S_{20,w}$ values of 1.120 (1.115, 1.123) *S* and 2.834 (2.789, 2.871) *S* respectively, and apparent M_w (S/D) value of 18.7 (18.2, 19.0) kDa for monomer (calculated M_w value is 16.0 kDa). Thus, gp41-shortNC has significantly less propensity to form trimers at neutral pH compared to gp41-longNC (Figure 4B) indicating that portions of the NHR and CHR contribute to oligomerization.

Overall, these results are in agreement with recent NMR studies with other gp41-based proteins in DPC micelles. Bax and coworkers reported that the gp41 ectodomain, with or without the immunodominant loop, dissociates into a monomer in the presence of detergents.[12] Two other reports on longer constructs, containing some or all of the membrane segments, have shown that these segments undergo monomer-trimer equilibria at high concentrations in DPC micelles at pH 4.[19,20] In our case, at lower protein concentrations (~5 μM), gp41-longNC, which is similar to the proteins $gp41^{1–194}$ and $gp41^{27–194}$ studied previously,[19,20] was found to be exclusively monomeric at pH 4 but undergoes a shift to trimer at neutral pHs.

We explored the capacity of gp41-longNC and gp41-shortNC to induce leakage of contents from POPC:POPG vesicles under several conditions ranging from pH 4 to 7 (Figures 3C and 4C, respectively). Since both proteins are stable only in the presence of detergent, samples were added in buffers containing small amounts of DPC (generally below 0.005%). Low concentrations of DPC were found to induce a minor amount of background liposome leakage and so data were normalized to DPC controls in all cases. Liposomal release for both proteins was highest relative to the DPC control at lower pHs (4 and 5) and significantly reduced at neutral pHs (6 and 7), although the pH-dependence was slightly attenuated for gp41-shortNC relative to gp41-longNC. In both cases, 100% leakage was observed at high protein concentrations (200 nM, corresponding to protein:lipid ratio of 0.002 for both gp41-longNC and gp41-shortNC) at pH 4, but this highest amount of leakage was reduced to ~20% and ~10% at pH 7. Intermediate pH conditions yielded intermediate levels of leakage. pH-Dependent fusogenic activity has previously been reported in gp41 constructs consisting of the FP and ectodomain, and has been attributed to electrostatic characteristics of these segments.[13,15,17] Both gp41-longNC and gp41-shortNC contain N- and C-terminal hexahistidine tags that may affect the overall charge and fusogenic activity. Multiple attempts to remove these tags by proteolysis were unsuccessful, since the proteins can only be stabilized in the presence of detergent that inactivates most common proteases. Instead, we performed the content release assays in 1 mM Zn^{2+} (10,000 times that of the protein concentration); the divalent cation is predicted to coordinate the histidine tags and prevent changes in protonation state. We found through NMR that the high concentration of Zn^{2+} can coordinate the histidine tags and weaken histidine tag NMR signals (data not shown). The leakage results were similar in the presence of Zn^{2+} at pH 4 (Figure S1, Supporting Information), indicating that protonation state of the histidine tag has no effect on fusogenic activity.

Roles of the Ectodomain, FP, and MPER-TM Segments

Comparison of the behavior of gp41-shortNC, and the two related deletion mutants, gp41-shortNC$^{\Delta FP}$ and gp41-shortNC$^{\Delta MTC}$, provides the opportunity to explore contributions of the FP and MPER-TM to structural stability. Previous work has suggested that the FP and MPER-TM segments may work alone or in concert to catalyze membrane fusion events.[32–38] The membrane-bound segments have been associated previously with membrane lytic activity,[13,38] and an X-ray structure of an "extended" six-helix bundle, containing segments of both the FP and MPER, suggests direct interactions between these two segments stabilize the post-fusion conformation.[39] Although segments of the FP and MPER-TM have been studied as isolated peptides, or together with larger constructs, their specific contributions to structure and function have not previously been explored in membrane environments. CD spectra indicate that gp41-shortNC$^{\Delta FP}$ and gp41-shortNC$^{\Delta MTC}$ are both α-helical in DPC, but that removal of the MPER-TM results in a significant loss of α-helical character, as expected (Figure 6A). The MPER-TM-C region alone (gp41-MTC) was significantly α-helical, matching previous reports of similar related variants. Both gp41-shortNC$^{\Delta FP}$ and gp41-MTC were monomeric by AUC (Figure S2, Supporting Information) and thus removal of the membrane segments did not affect the oligomerization state.

To explore the effects of the membrane segments on global structural stability, gp41-shortNC as well as both deletion mutants and gp41-MTC were all subjected to chemical denaturation with guanidinium hydrochloride (GdnHCl). The gp41-longNC construct was also included for comparison. Since all constructs were stabilized in the presence of DPC micelles, the effect of GdnHCl on micelle stability was first explored by dynamic light scattering (Table S1, Supporting information). We found that micelles were monodispersed of ~4 nm diameter, as expected for DPC,[40,41] up to GdnHCl concentrations of 5 M. At GdnHCl concentrations of higher than 5 M, the dynamic light scattering data quality was significantly affected by the substantial amount of GdnHCl, and it is not possible to determine if the DPC micelles are still intact. Therefore, definitive energetic analysis as is normally done for chemical denaturation was precluded. Nonetheless, general comparisons among unfolding trends should provide some insight into relative contributions of the membrane segments.

Gp41-longNC, gp41-shortNC, and gp41-shortNC$^{\Delta FP}$ could not be completely unfolded in 0.5% DPC (Figure 6B). Both gp41-shortNC and gp41-shortNC$^{\Delta FP}$ had mean residue ellipticity at 222 nm (θ_{222}) of −15,000 deg/dmol cm^2 without denaturant and at 7 M GdnHCl reached plateaus at −8,000 and −11,000 deg/dmol cm^2, respectively, indicating residual α-helicity. In contrast, gp41-shortNC$^{\Delta MTC}$ started at lower intensity negative θ_{222} values, consistent with less overall α-helicity, and reached a plateau of −2,000 deg/dmol cm^2 at high denaturant concentration, suggesting almost complete unfolding of gp41-shortNC$^{\Delta MTC}$. It is likely that the residual α-helicity of gp41-shortNC and gp41-shortNC$^{\Delta FP}$ at 7 M GdnHCl results from the MPER and/or TM, which are presumably buried in micelles and retain α-helical conformation in the presence of detergents despite high concentrations of chaotropic reagents. This is further confirmed by the denaturation profile of gp41-MTC which gives the least dynamic range of denaturation and that most of the secondary structure was retained

even at 7 M GdnHCl (Figure 6B). Secondary structure of membrane and transmembrane segments is not driven by hydrophobic interactions that are weakened by chaotropic agents. It was found in HIV-1 gp41 constructs and other α-helical transmembrane proteins that, even though their tertiary structures may be lost under chemical or thermal denaturing conditions, secondary structures of the transmembrane segments are typically retained within the membrane environment, considering the large energy penalty for the solvation of hydrophobic transmembrane helices.[31,42–44] Nonetheless, sigmoidal unfolding trends were observed for gp41-longNC, gp41-shortNC and gp41-shortNC$^{\Delta FP}$ with denaturation midpoints (C_Ms) of 5.7 M, 4.3 M and 1.8 M, respectively. The dynamic range for gp41-shortNC$^{\Delta MTC}$ was smaller since, at baseline (0 M GdnHCl), this variant had less α-helical character than the MPER-TM-C-containing constructs. Nonetheless, a sigmoidal unfolding trend was also observed with a C_M of 3.9 M. Lastly, gp41-MTC, the construct with the least denaturation dynamic range, shows a C_M of 2.1 M.

Binding to Broadly Neutralizing Antibodies (bNAbs)

The bNAbs 4E10, 2F5, Z13e1 and, most recently, 10E8 all target the MPER. Both 4E10 and 2F5 contain unusually long third heavy chain complementarity determining regions (CDRs) that cross-react with lipid environments[45] Structural studies of MPER peptides in membrane environments alone and in complex with the bNAbs have illustrated the structural plasticity of this region. The MPER forms a kinked α-helix structure in membrane,[16] an α-helix when bound to 4E10 and 10E8,[46,47] a β-loop when bound to 2F5,[48] and an S-shaped loop when bound to Z13e1.[49] We used biolayer interferometry to explore binding of 2F5 and 4E10 to gp41-longNC, gp41-shortNC, gp41-shortNC$^{\Delta FP}$ and gp41-shortNC$^{\Delta MTC}$ at pH 4 and pH 7 in DPC micelles (Table 1 and Figure S3, Supporting Information). Binding to gp41-shortNC$^{\Delta MTC}$ by either antibody was not observed (Figure S3, Supporting Information), which was expected since this construct does not contain the MPER sequence that is bound by both 4E10 and 2F5. Both 4E10 and 2F5 bound strongly to all constructs at pH 7, with dissociation constants in the single digit nanomolar range, consistent with previous reports.[11,50] However, both antibodies bound with much lower affinity at pH 4. In the case of 2F5, binding was reduced by ~100- to 4,000-fold; although less dramatic, reduction in binding was also observed with 4E10 (~3- to 20-fold).

DISCUSSION

A few recent studies have suggested that membrane- or detergent-bound HIV-1 gp41 can be present in monomeric form under certain conditions, and that the canonical core trimer, observed by X-ray crystallography, of the ectodomain lacking the membrane segments may not reflect the sole conformational preference of this subunit.[12,19,20] Our results are in general agreement with this observation and lend further evidence that dissociation to a monomeric form in detergents represents a relevant conformational preference of the fusion subunit. In addition, we discovered that the monomertrimer shift is affected by environmental pH for one of our constructs, gp41-longNC which contains the majority of the ectodomain and all of the membrane segments. Lytic activity, which we interpret as a proxy for fusogenic activity, is strongest at low pH for this construct suggesting that fusogenic activity is associated with the monomeric form. These results are consistent with

previous observations of pH-dependence of lipid mixing activity by similar gp41 constructs containing the ectodomain and the N-terminal fusion peptide, which showed hyper activity at pH 3 but negligible activity at pH 7.5.[30,51] However, we also note that gp41-shortNC, which contains less of the ectodomain and which we expect to be monomeric across a broad pH range, also exhibits a similar pH-dependent pattern of liposomal release. Therefore, the fusogenic activity may not be completely linked to a monomeric form of the protein.

Weliky and coworkers previously observed pH-dependent fusion activity in similar gp41 constructs containing the FP and ectodomain but lacking the MPER, TM, and C regions, and in this case the pH-dependence was ascribed to differential protonation states of ionizable residues that affect interaction with the membrane.[13,15,17] More recently, the pH-dependent fusion activity of gp41 variants was explored using vesicles with negative, neutral and positive charges; it was found that attractive electrostatic binding between gp41 residues and membrane vesicles are critical for protein-induced vesicle fusion.[18] These charged residues are also present in gp41-longNC and therefore may also be playing a role in pH-dependent behavior. The lipid composition of vesicles used in our studies contain only two components (POPC and POPG), with the phosphatidylcholine headgroup (POPC) as the major constituent as is the case with both plasma and HIV-1 viral membranes.[52] However, the effect of gp41-longNC and gp41-shortNC may differ with more complex membrane compositions, especially those containing headgroups with different charge characteristics and cholesterol. Our bulk leakage assay does not permit analysis of intermediate fusogenic effects; Weliky and coworkers have detected fast and slow fusion processes of vesicle fusion induced by ectodomain-containing constructs, and the fast process was attributed to protein monomers while the slow process to protein oligomers.[17] Although it is still not defined whether the monomeric or the oligomeric form of gp41 is physiologically relevant, their data agree with our observation that the liposomal leakage was most significantly induced by gp41 monomers at pH 4.

pH-Dependent fusogenic or conformational behavior has been observed in a number of fusion proteins, but generally this conditional behavior is associated with endosomal mechanisms of viral entry.[3,4,53–57] Although some reports suggest that some of the HIV-1 viral particle undergoes viral membrane fusion within endosomes (pH 4),[58] the majority of evidence indicates that fusion occurs at the plasma membrane (pH 7). Therefore, the direct relevance of the pH-dependent trimer dissociation and lytic activity described here and by others to membrane fusion during infection remains unclear.

Although several groups have documented a monomeric form of gp41 in detergent environments,[12,19,20] the topology of such a conformation in lipid bilayers remains elusive. In agreement with others, we have found that α-helical conformation is retained under conditions where the monomer is observed, thus suggesting, as proposed by Bax and coworkers, that dissociation of the independent NHR and CHR α-helices is one feature of this conformation. However, what is less clear is whether this form represents a compact, hairpin-like structure, an extended structure that potentially spans two micelles (FP in one and MPER-TM in the other), or some dynamic equilibrium of the two. In either case, the exposure of hydrophobic patches on the NHR and CHR, that would constitute the interhelical binding grooves for formation of the six-helix bundle, is predicted to result in an

extended surface for potential membrane interactions. It is plausible that interaction of the hydrophobic regions promote the leakage activity shown here and potentially biological fusogenic activity during natural infection. Amphipathic α-helices in general can have membrane disrupting activities that is dependent on local secondary structure. Antimicrobial peptides such as magainin are prime examples of this phenomenon.[59] While it is possible that this feature does contribute to the mechanism of membrane fusion, it is somewhat inconsistent with the prevailing notion that fusion of the two membranes is completely dependent on folding of the six-helix bundle to overcome the kinetic barrier associated with bringing the two membranes together. Furthermore, while we have demonstrated strong leakage activity here, generally these occur at nanomolar concentrations, and the spike density on an individual HIV-1 particle is relatively low. The number of spikes required for HIV-1 infection has not been precisely defined.[60] Some models estimate eight spikes are needed for membrane fusion,[60] but it has also been suggested that as few as two spikes may be required.[61] Therefore, while the bulk liposome release assays shown here provide some behavioral characterization of the protein, such characteristics may play only a partial role in the actual membrane fusion reaction.

Earlier work has suggested interaction of the MPER segment with the FP may play a role in late-stage fusion events by direct interaction with one another.[33,39] Our results indicated that, within the context of gp41-shortNC, both of these segments do contribute to the structural stability. Weissenhorn and coworkers previously reported the X-ray structure of an “extended” six-helix bundle, consisting of major elements of the NHR and CHR as well as segments of the MPER and FP.[39] They found that this extended gp41 six-helix bundle has a higher melting temperature than does a related analog lacking the MPER and FP segments, and that the X-ray structure indicated direct residue-to-residue contacts between these segments. Here, we have found that the FP and MPER/TM segments serve to stabilize the structure of gp41-shortNC, as deletion of either one increases susceptibility to GdnHCl denaturation. However, since gp41-shortNC is monomeric under these conditions, many of the residue-to-residue specific interactions that serve to stabilize the six-helix bundle are likely not relevant here, although we cannot rule out that each monomer forms a folded-back hairpin conformation which would allow the MPER and FP to be in proximity to one another and thus interact. An alternative possibility is that both of these segments serve to promote secondary structure in a monomeric membrane-bound form, potentially nucleated by interactions with membrane. This would explain why deletion of either segment is seemingly non-equivalent, with deletion of the FP having a more significant effect on stability.

Gp41 is the target of both fusion inhibitory peptides and MPER-specific bNAbs. We find that two such bNAbs, 4E10 and 2F5, bind tightly to gp41 presented within the context of the micelle environment at neutral pH, but that binding was reduced at low pH. The fact that the binding was comparable for all three constructs containing the MPER (gp41-longNC, gp41-shortNC, and gp41-shortNC$^{\Delta FP}$) suggests that presentation of the critical neutralization epitopes within context of shorter-or longer-mimics of the ectodomain do not have a substantial effect on binding affinity. Previous reports have demonstrated that presentation of the MPER in either membrane environments, or as fusions to the transmembrane domain embedded in membrane environments, is a critical aspect of recognition by these two

antibodies.[10,11,16,45,46] The novel insight provided by our binding studies is that affinity is not affected by inclusion of additional portions of the ectodomain or fusion peptide region.

Our data also suggests that the MPER epitopes can be engaged by bNAbs 4E10 and 2F5 within the context of well-folded micelle-embedded gp41 variants, gp41-longNC and gp41-shortNC, at pH 7 with single-digit nanomolar affinity. There has been some debate about whether the MPER epitope is presented in a conformation relevant to virus neutralization when included as part of the folded gp41 ectodomain. Chen and coworkers reported that 4E10 and 2F5 can bind designed proteins that mimic the gp41 extended intermediate ("gp41-inter", and "GCN4-gp41-inter"), in which the CHR segment preceding the MPER is not complexed with the NHR, but not to the folded ectodomain containing both the NHR and CHR which is presumably representative of the post-fusion six-helix bundle conformation.[62,63] However, two other reports have shown that folded gp41 core ectodomain constructs containing the NHR, CHR, and the MPER exhibit tight binding with 4E10 and 2F5.[18,64] Our results indicate that micelle-embedded constructs containing major elements of the ectodomain indeed are recognized by 2F5 and 4E10 and, in the case of gp41-longNC, under conditions where the protein is trimeric. However, in the case of gp41-longNC, it is not known if the NHR and CHR adopt a six-helix bundle conformation.

The cause for the large drop in binding affinity for both 2F5 and 4E10 at pH 4 is not clear. This recognition difference is most dramatic in the case of 2F5 for binding to gp41-longNC (4,000-fold difference in K_D at pHs 4 and 7), and may reflect the difference in oligomerization state we have observed for this protein between the two pH conditions in micelles. Consistent with this conclusion is the fact that the effect of pH was much stronger for both 2F5 and 4E10 for binding to gp41-longNC (4,000- and 30-fold difference, respectively) than either gp41-shortNC or gp41-shortNC$^{\Delta FP}$, which are monomeric at both pH 4 and 7, despite the fact that binding to all three constructs was similar at pH 7 for both antibodies. The gp41-longNC trimer at pH 7 would contain three local copies of the MPER and therefore could give rise to an avidity effect. Additionally, there may be different conformational preferences of the MPER in the context of the pH 4 monomer and the pH 7 trimer with the latter being more relevant to binding by 2F5 and 4E10. There was still a difference in binding at pH 4 and pH 7 for gp41-shortNC or gp41-shortNC$^{\Delta FP}$ for both 2F5 and 4E10, but this difference was less dramatic than observed for gp41-longNC. Therefore, another possibility is that the low pH could attenuate the electrostatic interactions between the gp41 constructs and the antibodies, considering that there are extensive hydrogen bond and salt bridge contacts at both binding interfaces.[46,48] It is also possible that some local secondary structural changes in the MPER that affect binding or its interaction with DPC was induced at low pH. It has been demonstrated previously that the structural stability of MPER peptide is pH-dependent, with significant disorder at neutral pH particularly for the residues near and including the 2F5 epitope.[65] A final possibility is that these pH-induced effects affect the antibody structure.

Together, our results support recent reports suggesting the HIV-1 gp41 subunit can dissociate to a monomeric form in membrane environments, here as a result of changes in pH. Since this monomeric species is associated with functional activity (membrane lysis) and remains well behaved in DPC micelles with substantial secondary structure, it seems

unlikely that this state represents a globally unfolded or inactivated form of the protein. Instead, our results in conjunction with those from other groups strongly imply that the monomeric form could represent a novel conformational state, though whether this is a mimic of a late-stage fusion intermediate remains to be determined. The fact that 2F5 and 4E10, two antibodies that are postulated to inhibit membrane fusion, recognize gp41-longNC under monomeric pH 4 conditions, but with substantially lower activity, suggests that at least the MPER region is not in a fusion relevant conformation in this state. Nonetheless, these results indicate that potentially multiple pathways or new intermediates for gp41-directed membrane fusion may exist and merit further examination.

Supplementary Material

Refer to Web version on PubMed Central for supplementary material.

Acknowledgments

FUNDING STATEMENT: This work was funded by the National Institutes of Health (AI090249 to J. R. L., GM072085 to M. E. G.).

ABBREVIATIONS

ANTS	8-aminonapthalene-1,3,6 trisulfonic acid
AUC	analytical ultracentrifugation
bNAbs	broadly neutralizing antibodies
CHR	C-terminal heptad repeat
CD	circular dichroism
CDR	complementarity determining region
DPC	n-dodecylphosphocholine
DPX	*p*-xylene-bis-pyridinium bromide
DSS	4,4-dimethyl-4-silapentane-1-sulfonic acid
FP	fusion peptide
IPTG	isopropyl β-D-1-thiogalactopyranoside
NHR	N-terminal heptad repeat
Ni-NTA	Ni-Nitrilotriacetic acid
GdnHCl	guanadinium hydrochlodride
k_a	association rate constant
k_d	dissociation rate constant
K_D	equilibrium dissociation constant
MPER	membrane proximal external region

PBS	phosphate buffered saline
POPC	1-palmitoyl-2-oleoyl-sn-glycero-3-phosphocholine
POPG	1-palmitoyl-2-oleoyl-sn-glycero-3-phosphoglycerol
TM	transmembrane domain

References

1. Chan DC, Fass D, Berger JM, Kim PS. Core structure of gp41 from the HIV envelope glycoprotein. Cell. 1997; 89:263–273. [PubMed: 9108481]
2. Eckert DM, Kim PS. Mechanisms of viral membrane fusion and its inhibition. Annu Rev Biochem. 2001; 70:777–810. [PubMed: 11395423]
3. Harrison SC. Mechanism of membrane fusion by viral envelope proteins. Adv Virus Res. 2005; 64:231–261. [PubMed: 16139596]
4. Harrison SC. Viral membrane fusion. Nat Struct Mol Biol. 2008; 15:690–698. [PubMed: 18596815]
5. Weissenhorn W, Dessen A, Harrison SC, Skehel JJ, Wiley DC. Atomic structure of the ectodomain from HIV-1 gp41. Nature. 1997; 387:426–430. [PubMed: 9163431]
6. White JM, Delos SE, Brecher M, Schornberg K. Structures and mechanisms of viral membrane fusion proteins: Multiple variations on a common theme. Crit Rev Biochem Mol Biol. 2008; 43:189–219. [PubMed: 18568847]
7. Cardone G, Brecher M, Fontana J, Winkler DC, Butan C, White JM, Stevena AC. Visualization of the Two-Step Fusion Process of the Retrovirus Avian Sarcoma/Leukosis Virus by Cryo-Electron Tomography. J Virol. 2012; 86:12129–12137. [PubMed: 22933285]
8. Kim YH, Donald JE, Grigoryan G, Leser GP, Fadeev AY, Lamb RA, DeGrado WF. Capture and imaging of a prehairpin fusion intermediate of the paramyxovirus PIV5. Proc Natl Acad Sci U S A. 2011; 108:20992–20997. [PubMed: 22178759]
9. Markosyan RM, Cohen FS, Melikyan GB. HIV-1 envelope proteins complete their folding into six-helix bundles immediately after fusion pore formation. Mol Biol Cell. 2003; 14:926–938. [PubMed: 12631714]
10. Montero M, Gulzar N, Klaric KA, Donald JE, Lepik C, Wu S, Tsai S, Julien JP, Hessell AJ, Wang SX, Lu S, Burton DR, Pai EF, DeGrado WF, Scott JK. Neutralizing Epitopes in the Membrane-Proximal External Region of HIV-1 gp41 Are Influenced by the Transmembrane Domain and the Plasma Membrane. J Virol. 2012; 86:2930–2941. [PubMed: 22238313]
11. Reardon PN, Sage H, Dennison SM, Martin JW, Donald BR, Alam SM, Haynes BF, Spicer LD. Structure of an HIV-1-neutralizing antibody target, the lipid-bound gp41 envelope membrane proximal region trimer. Proc Natl Acad Sci U S A. 2014; 111:1391–1396. [PubMed: 24474763]
12. Roche J, Louis JM, Grishaev A, Ying JF, Bax A. Dissociation of the trimeric gp41 ectodomain at the lipid-water interface suggests an active role in HIV-1 Env-mediated membrane fusion. Proc Natl Acad Sci U S A. 2014; 111:3425–3430. [PubMed: 24550514]
13. Sackett K, Nethercott MJ, Epand RF, Epand RM, Kindra DR, Shai Y, Weliky DP. Comparative Analysis of Membrane-Associated Fusion Peptide Secondary Structure and Lipid Mixing Function of HIV gp41 Constructs that Model the Early Pre-Hairpin Intermediate and Final Hairpin Conformations. J Mol Biol. 2010; 397:301–315. [PubMed: 20080102]
14. Sackett K, Nethercott MJ, Zheng ZX, Weliky DP. Solid-State NMR Spectroscopy of the HIV gp41 Membrane Fusion Protein Supports Intermolecular Antiparallel 13 Sheet Fusion Peptide Structure in the Final Six-Helix Bundle State. J Mol Biol. 2014; 426:1077–1094. [PubMed: 24246500]
15. Sackett K, TerBush A, Weliky DP. HIV gp41 six-helix bundle constructs induce rapid vesicle fusion at pH 3.5 and little fusion at pH 7.0: understanding pH dependence of protein aggregation, membrane binding, and electrostatics, and implications for HIV-host cell fusion. Eur Biophys J. 2011; 40:489–502. [PubMed: 21222118]

16. Sun ZYJ, Oh KJ, Kim MY, Yu J, Brusic V, Song LK, Qiao ZS, Wang JH, Wagner G, Reinherz EL. HIV-1 broadly neutralizing antibody extracts its epitope from a kinked gp41 ectodomain region on the viral membrane. Immunity. 2008; 28:52–63. [PubMed: 18191596]
17. Ratnayake PU, Sackett K, Nethercott MJ, Weliky DP. pH-dependent vesicle fusion induced by the ectodomain of the human immunodeficiency virus membrane fusion protein gp41: Two kinetically distinct processes and fully-membrane-associated gp41 with predominant β sheet fusion peptide conformation. Biochim Biophys Acta. 2015; 1848:289–298. [PubMed: 25078440]
18. Banerjee K, Weliky DP. Folded Monomers and Hexamers of the Ectodomain of the HIV gp41 Membrane Fusion Protein: Potential Roles in Fusion and Synergy Between the Fusion Peptide, Hairpin, and Membrane-Proximal External Region. Biochemistry. 2014; 53:7184–7198. [PubMed: 25372604]
19. Lakomek NA, Kaufman JD, Stahl SJ, Louis JM, Grishaev A, Wingfield PT, Bax A. Internal Dynamics of the Homotrimeric HIV-1 Viral Coat Protein gp41 on Multiple Time Scales. Angew Chem Int Ed. 2013; 52:3911–3915.
20. Lakomek NA, Kaufman JD, Stah SJ, Wingfield PT. HIV-1 Envelope Protein gp41: An NMR Study of Dodecyl Phosphocholine Embedded gp41 Reveals a Dynamic Prefusion Intermediate Conformation. Structure. 2014; 22:1311–1321. [PubMed: 25132083]
21. Tamm LK, Lee J, Liang B. Capturing glimpses of an elusive HIV gp41 prehairpin fusion intermediate. Structure. 2014; 22:1225–1226. [PubMed: 25185826]
22. Louis-Jeune C, Andrade-Navarro MA, Perez-Iratxeta C. Prediction of protein secondary structure from circular dichroism using theoretically derived spectra (vol 80, pg 374, 2012). Proteins: Struct, Funct, Bioinf. 2012; 80:2818–2818.
23. Korendovych IV, Senes A, Kim YH, Lear JD, Fry HC, Therien MJ, Blasie JK, Walker FA, Degrado WF. De novo design and molecular assembly of a transmembrane diporphyrin-binding protein complex. J Am Chem Soc. 2010; 132:15516–15518. [PubMed: 20945900]
24. Tanford C, Nozaki Y, Reynolds JA, Makino S. Molecular characterization of proteins in detergent solutions. Biochemistry. 1974; 13:2369–2376. [PubMed: 4364776]
25. Tanford C, Reynolds JA. Characterization of membrane proteins in detergent solutions. Biochim Biophys Acta. 1976; 457:133–170. [PubMed: 135582]
26. Philo JS. Improved methods for fitting sedimentation coefficient distributions derived by time-derivative techniques. Anal Biochem. 2006; 354:238–246. [PubMed: 16730633]
27. Stafford WF. Boundary Analysis in Sedimentation Transport Experiments – a Procedure for Obtaining Sedimentation Coefficient Distributions Using the Time Derivative of the Concentration Profile. Anal Biochem. 1992; 203:295–301. [PubMed: 1416025]
28. Delaglio F, Grzesiek S, Vuister GW, Zhu G, Pfeifer J, Bax A. Nmrpipe – a Multidimensional Spectral Processing System Based on Unix Pipes. J Biomol NMR. 1995; 6:277–293. [PubMed: 8520220]
29. Tan K, Liu J, Wang J, Shen S, Lu M. Atomic structure of a thermostable subdomain of HIV-1 gp41. Proc Natl Acad Sci U S A. 1997; 94:12303–12308. [PubMed: 9356444]
30. Lev N, Fridmann-Sirkis Y, Blank L, Bitler A, Epand RF, Epand RM, Shai Y. Conformational Stability and Membrane Interaction of the Full-Length Ectodomain of HIV-1 gp41: Implication for Mode of Action†. Biochemistry. 2009; 48:3166–3175. [PubMed: 19206186]
31. Sackett K, Nethercott MJ, Shai Y, Weliky DP. Hairpin Folding of HIV gp41 Abrogates Lipid Mixing Function at Physiologic pH and Inhibits Lipid Mixing by Exposed gp41 Constructs. Biochemistry. 2009; 48:2714–2722. [PubMed: 19222185]
32. Quintana FJ, Gerber D, Kent SC, Cohen IR, Shai Y. HIV-1 fusion peptide targets the TCR and inhibits antigen-specific T cell activation. J Clin Invest. 2005; 115:2149–2158. [PubMed: 16007266]
33. Reuven EM, Dadon Y, Viard M, Manukovsky N, Blumenthal R, Shai Y. HIV-1 gp41 Transmembrane Domain Interacts with the Fusion Peptide: Implication in Lipid Mixing and Inhibition of Virus-Cell Fusion. Biochemistry. 2012; 51:2867–2878. [PubMed: 22413880]
34. Bloch I, Quintana FJ, Gerber D, Cohen T, Cohen IR, Shai Y. T-cell inactivation and immunosuppressive activity induced by HIV gp41 via novel interacting motif. FASEB J. 2007; 21:393–401. [PubMed: 17185749]

35. Cohen T, Pevsner-Fischer M, Cohen N, Cohen IR, Shai Y. Characterization of the interacting domain of the HIV-1 fusion peptide with the transmembrane domain of the T-cell receptor. Biochemistry. 2008; 47:4826–4833. [PubMed: 18376816]
36. Shang L, Yue L, Hunter E. Role of the membrane-spanning domain of human immunodeficiency virus type 1 envelope glycoprotein in cell-cell fusion and virus infection. J Virol. 2008; 82:5417–5428. [PubMed: 18353944]
37. Cohen T, Cohen SJ, Antonovsky N, Cohen IR, Shai Y. HIV-1 gp41 and TCRalpha trans-membrane domains share a motif exploited by the HIV virus to modulate T-cell proliferation. PLoS Path. 2010; 6:e1001085.
38. Lai AL, Moorthy AE, Li YL, Tamm LK. Fusion Activity of HIV gp41 Fusion Domain Is Related to Its Secondary Structure and Depth of Membrane Insertion in a Cholesterol-Dependent Fashion. J Mol Biol. 2012; 418:3–15. [PubMed: 22343048]
39. Buzon V, Natrajan G, Schibli D, Campelo F, Kozlov MM, Weissenhorn W. Crystal Structure of HIV-1 gp41 Including Both Fusion Peptide and Membrane Proximal External Regions. PLoS Path. 2010; 6:e1000880.
40. Lipfert J, Columbus L, Chu VB, Lesley SA, Doniach S. Size and shape of detergent micelles determined by small-angle X-ray scattering. J Phys Chem B. 2007; 111:12427–12438. [PubMed: 17924686]
41. Wymore T, Gao XF, Wong TC. Molecular dynamics simulation of the structure and dynamics of a dodecylphosphocholine micelle in aqueous solution. J Mol Struct. 1999; 485:195–210.
42. Lau FW, Bowie JU. A method for assessing the stability of a membrane protein. Biochemistry. 1997; 36:5884–5892. [PubMed: 9153430]
43. Schlebach JP, Peng D, Kroncke BM, Mittendorf KF, Narayan M, Carter BD, Sanders CR. Reversible folding of human peripheral myelin protein 22, a tetraspan membrane protein. Biochemistry. 2013; 52:3229–3241. [PubMed: 23639031]
44. Bowie JU. Membrane proteins: a new method enters the fold. Proc Natl Acad Sci U S A. 2004; 101:3995–3996. [PubMed: 15024105]
45. Haynes BF, Fleming J, St Clair EW, Katinger H, Stiegler G, Kunert R, Robinson J, Scearce RM, Plonk K, Staats HF, Ortel TL, Liao HX, Alam SM. Cardiolipin polyspecific autoreactivity in two broadly neutralizing HIV-1 antibodies. Science. 2005; 308:1906–1908. [PubMed: 15860590]
46. Cardoso RMF, Zwick MB, Stanfield RL, Kunert R, Binley JM, Katinger H, Burton DR, Wilson IA. Broadly neutralizing anti-HIV antibody 4E10 recognizes a helical conformation of a highly conserved fusion-associated motif in gp41. Immunity. 2005; 22:163–173. [PubMed: 15723805]
47. Huang JH, Ofek G, Laub L, Louder MK, Doria-Rose NA, Longo NS, Imamichi H, Bailer RT, Chakrabarti B, Sharma SK, Alam SM, Wang T, Yang YP, Zhang BS, Migueles SA, Wyatt R, Haynes BF, Kwong PD, Mascola JR, Connors M. Broad and potent neutralization of HIV-1 by a gp41-specific human antibody. Nature. 2012; 491:406–412. [PubMed: 23151583]
48. Ofek G, Tang M, Sambor A, Katinger H, Mascola JR, Wyatt R, Kwong PD. Structure and mechanistic analysis of the anti-human immunodeficiency virus type 1 antibody 2F5 in complex with its gp41 epitope. J Virol. 2004; 78:10724–10737. [PubMed: 15367639]
49. Pejchal R, Gach JS, Brunel FM, Cardoso RM, Stanfield RL, Dawson PE, Burton DR, Zwick MB, Wilson IA. A conformational switch in human immunodeficiency virus gp41 revealed by the structures of overlapping epitopes recognized by neutralizing antibodies. J Virol. 2009; 83:8451–8462. [PubMed: 19515770]
50. Brunel FM, Zwick MB, Cardoso RMF, Nelson JD, Wilson IA, Burton DR, Dawson PE. Structure-function analysis of the epitope for 4E10, a broadly neutralizing human immunodeficiency virus type 1 antibody. J Virol. 2006; 80:1680–1687. [PubMed: 16439525]
51. Vogel EP, Curtis-Fisk J, Young KM, Weliky DP. Solid-State Nuclear Magnetic Resonance (NMR) Spectroscopy of Human Immunodeficiency Virus gp41 Protein That Includes the Fusion Peptide: NMR Detection of Recombinant Fgp41 in Inclusion Bodies in Whole Bacterial Cells and Structural Characterization of Purified and Membrane-Associated Fgp41. Biochemistry. 2011; 50:10013–10026. [PubMed: 21985645]

52. Lorizate M, Sachsenheimer T, Glass B, Habermann A, Gerl MJ, Kräusslich HG, Brügger B. Comparative lipidomics analysis of HIV-1 particles and their producer cell membrane in different cell lines. Cell Microbiol. 2013; 15:292–304. [PubMed: 23279151]

53. Koellhoffer JF, Dai Z, Malashkevich VN, Stenglein MD, Liu Y, Toro R, J SH, Chandran K, DeRisi JL, Almo SC, Lai JR. Structural characterization of the glycoprotein GP2 core domain from the CAS virus, a novel arenavirus-like species. J Mol Biol. 2014; 426:1452–1468. [PubMed: 24333483]

54. Regula LK, Harris R, Wang F, Higgins CD, Koellhoffer JF, Zhao Y, Chandran K, Gao J, Girvin ME, Lai JR. Conformational properties of peptides corresponding to the ebolavirus GP2 membrane-proximal external region in the presence of micelle-forming surfactants and lipids. Biochemistry. 2013; 52:3393–3404. [PubMed: 23650881]

55. Koellhoffer JF, Malashkevich VN, Harrison JS, Toro R, Bhosle RC, Chandran K, Almo SC, Lai JR. Crystal structure of the Marburg virus GP2 core domain in its postfusion conformation. Biochemistry. 2012; 51:7665–7675. [PubMed: 22935026]

56. Harrison JS, Koellhoffer JF, Chandran K, Lai JR. Marburg virus glycoprotein GP2: pH-dependent stability of the ectodomain alpha-helical bundle. Biochemistry. 2012; 51:2515–2525. [PubMed: 22369502]

57. Harrison JS, Higgins CD, Chandran K, Lai JR. Designed protein mimics of the Ebola virus glycoprotein GP2 alpha-helical bundle: stability and pH effects. Protein Science. 2011; 20:1587–1596. [PubMed: 21739501]

58. Miyauchi K, Kim Y, Latinovic O, Morozov V, Melikyan GB. HIV Enters Cells via Endocytosis and Dynamin-Dependent Fusion with Endosomes. Cell. 2009; 137:433–444. [PubMed: 19410541]

59. Zasloff M. Antimicrobial peptides of multicellular organisms. Nature. 2002; 415:389–395. [PubMed: 11807545]

60. Magnus C, Rusert P, Bonhoeffer S, Trkola A, Regoes RR. Estimating the Stoichiometry of Human Immunodeficiency Virus Entry. J Virol. 2009; 83:1523–1531. [PubMed: 19019953]

61. Yang XZ, Kurteva S, Ren XP, Lee S, Sodroski J. Subunit stoichiometry of human immunodeficiency virus type 1 envelope glycoprotein trimers during virus entry into host cells. J Virol. 2006; 80:4388–4395. [PubMed: 16611898]

62. Frey G, Chen J, Rits-Volloch S, Freeman MM, Zolla-Pazner S, Chen B. Distinct conformational states of HIV-1 gp41 are recognized by neutralizing and non-neutralizing antibodies. Nat Struct Mol Biol. 2010; 17:1486–1491. [PubMed: 21076402]

63. Frey G, Peng H, Rits-Volloch S, Morelli M, Cheng Y, Chen B. A fusion-intermediate state of HIV-1 gp41 targeted by broadly neutralizing antibodies. Proc Natl Acad Sci U S A. 2008; 105:3739–3744. [PubMed: 18322015]

64. Wang J, Tong P, Lu L, Zhou L, Xu L, Jiang S, Chen Y-h. HIV-1 gp41 Core with Exposed Membrane-Proximal External Region Inducing Broad HIV-1 Neutralizing Antibodies. PLoS One. 2011; 6:e18233. [PubMed: 21483871]

65. Coutant J, Yu H, Clément MJ, Alfsen A, Toma F, Curmi PA, Bomsel M. Both lipid environment and pH are critical for determining physiological solution structure of 3-D-conserved epitopes of the HIV-1 gp41-MPER peptide P1. FASEB J. 2008; 22:4338–4351. [PubMed: 18776068]

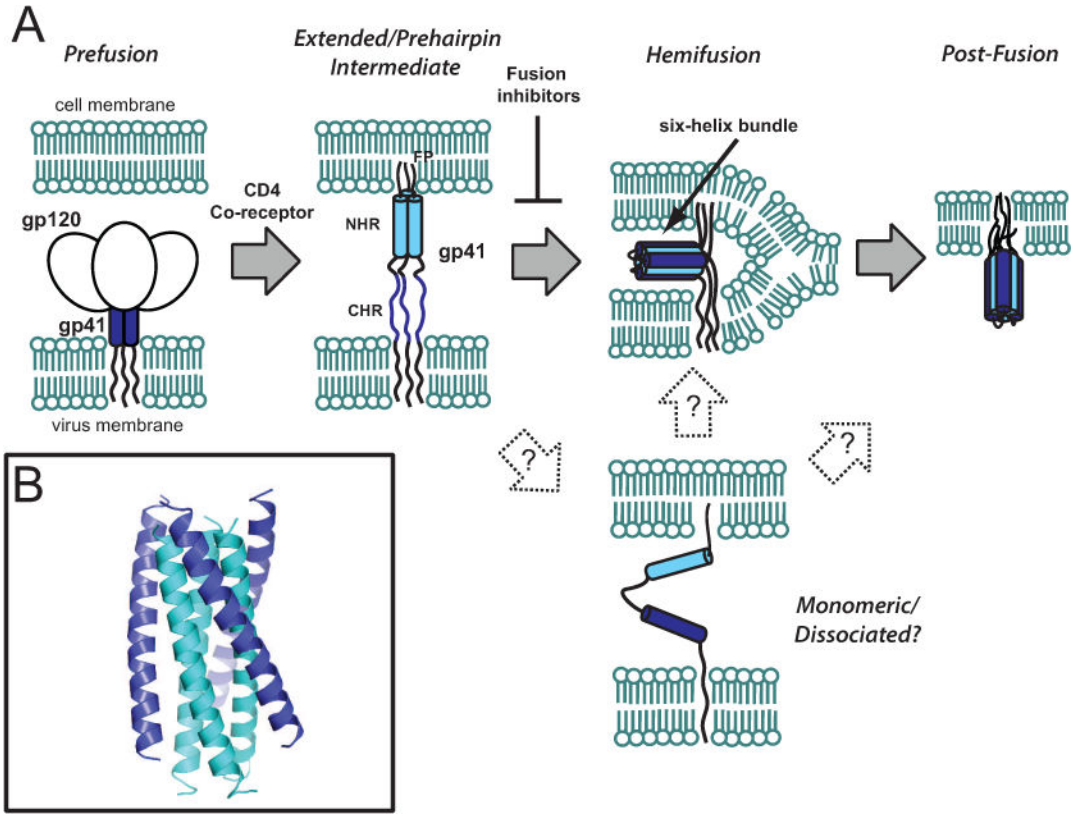

Figure 1. Role of the HIV-1 gp41 fusion subunit in viral membrane fusion

(A) Proposed mechanism of viral membrane fusion mediated by gp120 and gp41. A putative monomeric/dissociated intermediate has been proposed as a late-stage intermediate. Although drawn as a strict monomer here, potentially this intermediate could also be trimeric as mediated by the MPER and TM segments. (B) X-ray structure of the six-helix bundle (PDB IDs 1AIK and 1ENV, with 1AIK shown here) formed by the NHR (cyan) and CHR (blue) segments.

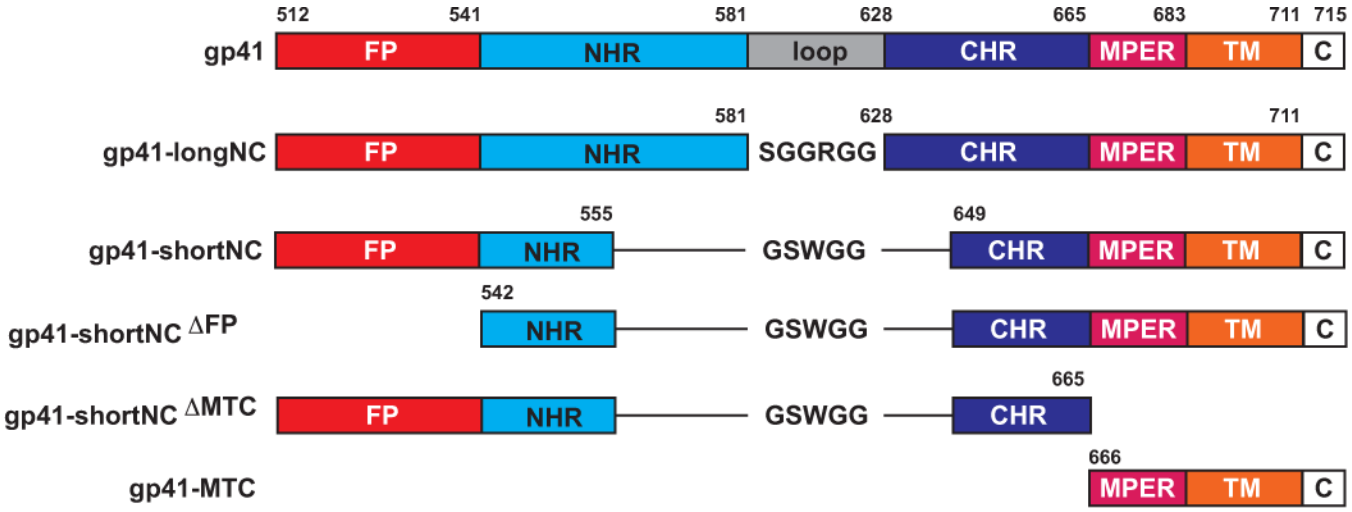

Figure 2. Schematic of HIV-1 gp41 and constructs studied

FP, fusion peptide; NHR, N-heptad repeat region; CHR, C-heptad repeat region; MPER, membrane-proximal external region; TM, transmembrane region; C, C-terminal tail. HXB2 numbering is shown.

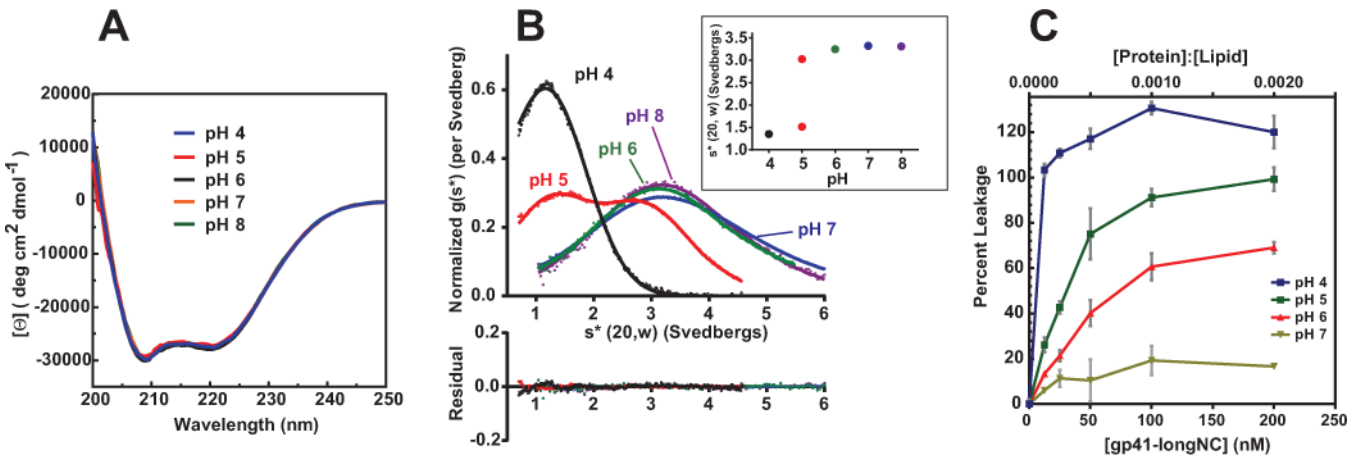

Figure 3. Properties of gp41-longNC

CD (A), AUC (B), and liposome release assay (C) under various pH conditions. For AUC, a monomeric species was observed at low pH (pH 4) and trimeric species at higher pHs (pH 6, 7 and 8). At pH 5, both monomeric and trimeric species were observed, illustrated in the inset. All AUC experiments were performed at 4 – 5 μM protein concentrations.

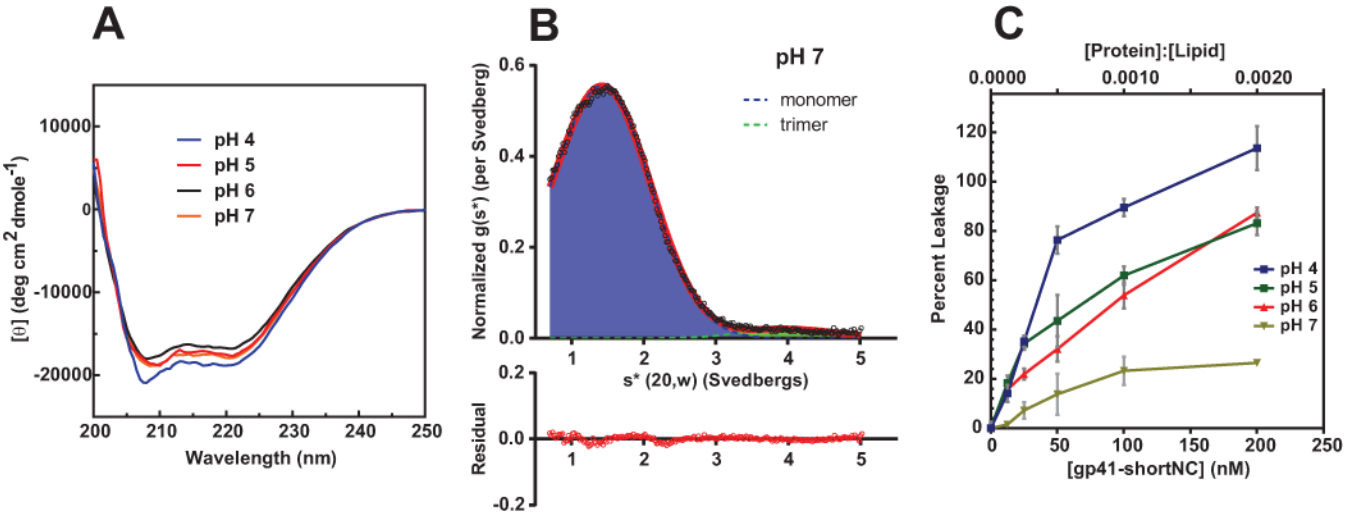

Figure 4. Properties of gp41-shortNC

CD (A) and AUC (B) at pH 7, and liposome release assay (C) under various pH conditions. For AUC data obtained at 21 μM gp41-shortNC (pH 7), the contributions from monomer and trimer are depicted in blue and green, respectively.

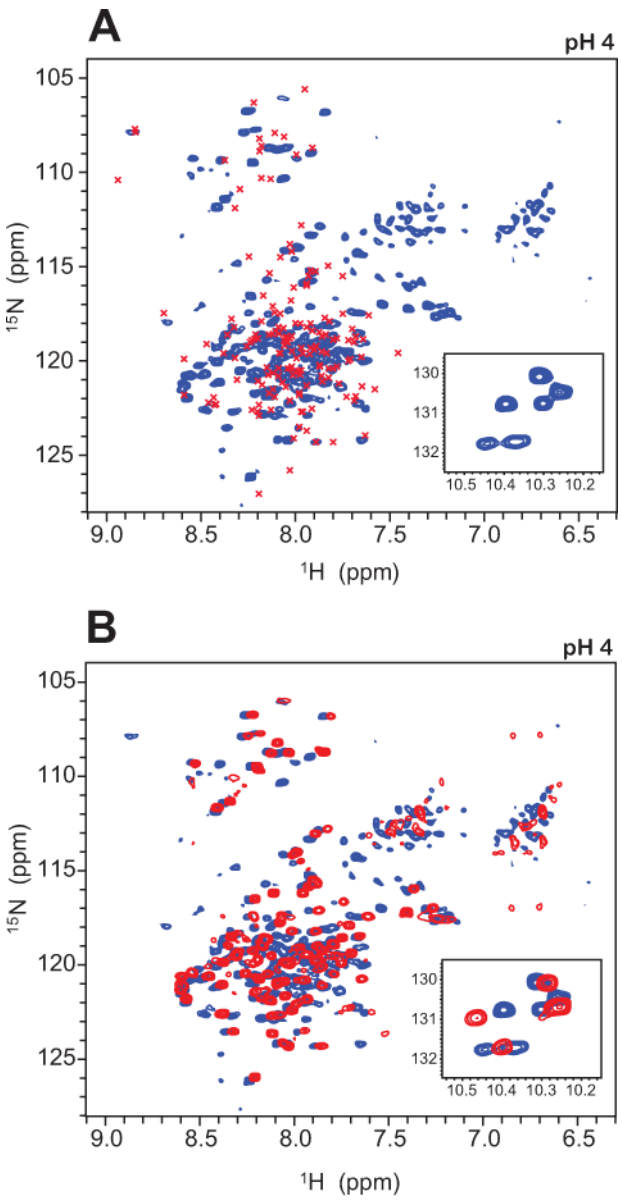

Figure 5. ^{1}H^{15}N TROSY spectra of gp41-longNC and gp41-shortNC at pH 4

(A) TROSY spectrum of gp41-longNC (blue). Trp side chain region of the spectra are shown as insets. Previously reported cross peak positions for similar gp41 constructs[12,19] are indicated in red cross. (B) Overlay of the TROSY spectra for gp41-longNC (blue) and gp41-shortNC (red). 90% of the gp41-shortNC cross peaks fall near or on the corresponding resonance in the gp41-longNC.

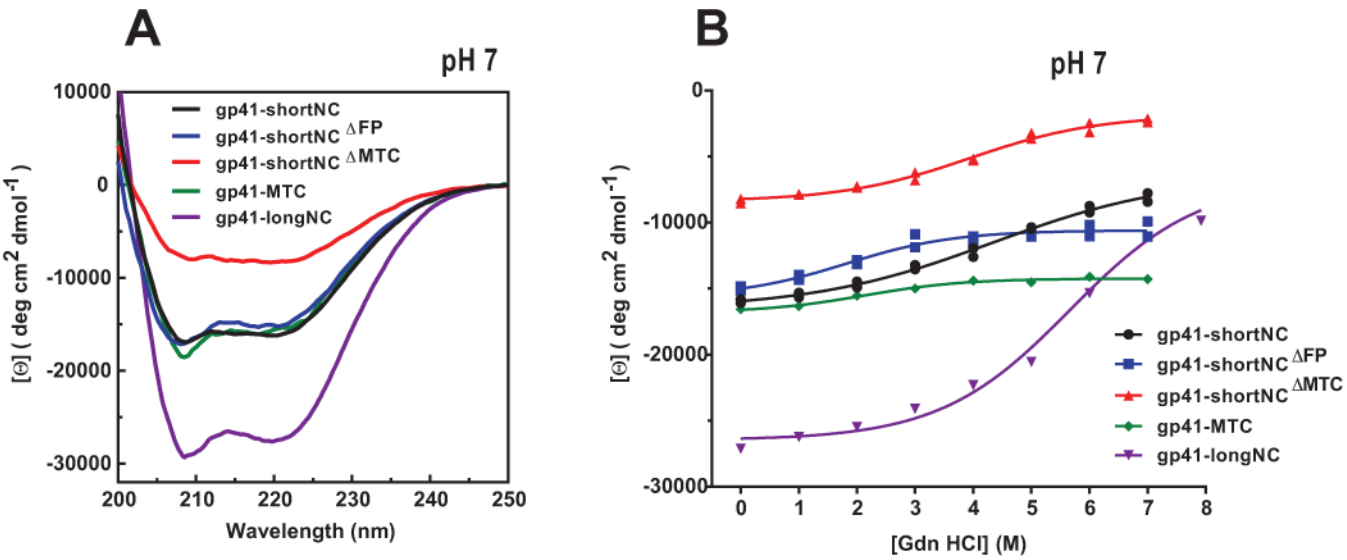

Figure 6. CD and chemical denaturation of gp41-shortNC, gp41-shortNC$^{\Delta FP}$, gp41-shortNC$^{\Delta MTC}$, gp41-MTC, and gp41-longNC at pH 7

(A) CD wavelength scans for gp41-shortNC$^{\Delta FP}$, gp41-shortNC$^{\Delta MTC}$, and gp41-MTC with data for gp41-shortNC and gp41-longNC included for comparison; (B) chemical denaturation of all five constructs.

Table 1

Biolayer interferometry binding measurements.

		2F5			4E10		
Construct:	**Conditions**	k_a (M^{-1} s^{-1})	k_d (s^{-1})	K_D (nM)	k_a (M^{-1} s^{-1})	k_d (s^{-1})	K_D (nM)
gp41-longNC	pH 4	1.2×10^3	9.5×10^{-3}	8000	1.0×10^4	1.3×10^{-3}	130
	pH 7	2.0×10^5	4.0×10^{-4}	2.0	1.2×10^5	5.1×10^{-4}	4.4
gp41-shortNC	pH 4	1.3×10^4	2.8×10^{-3}	210	5.5×10^4	6.5×10^{-4}	12
	pH 7	2.7×10^5	6.2×10^{-4}	2.3	1.9×10^5	6.3×10^{-4}	3.4
gp41-shortNC$^{\Delta FP}$	pH 4	1.5×10^4	7.5×10^{-3}	500	8.4×10^4	2.3×10^{-3}	28
	pH 7	4.5×10^5	1.4×10^{-3}	3.1	3.2×10^5	9.3×10^{-4}	2.9